IOPscience

HOME | SEARCH | PACS & MSC | JOURNALS | ABOUT | CONTACT US

Transport of an arbitrary near-field component with an array of tilted wires

This article has been downloaded from IOPscience. Please scroll down to see the full text article.

2009 New J. Phys. 11 083023

(http://iopscience.iop.org/1367-2630/11/8/083023)

The Table of Contents and more related content is available

Download details:
IP Address: 193.136.94.30
The article was downloaded on 20/08/2009 at 14:06

Please note that terms and conditions apply.

New Journal of Physics
The open-access journal for physics

Transport of an arbitrary near-field component with an array of tilted wires

Tiago A Morgado and Mário G Silveirinha[1]
Departamento de Engenharia Electrotécnica, Universidade de Coimbra, Instituto de Telecomunicações, Pólo II, 3030 Coimbra, Portugal
E-mail: mario.silveirinha@co.it.pt

New Journal of Physics **11** (2009) 083023 (21pp)
Received 30 April 2009
Published 19 August 2009
Online at http://www.njp.org/
doi:10.1088/1367-2630/11/8/083023

Abstract. In this work, we investigate the possibility of near-field transport using an array of tilted metallic wires. It is demonstrated that consistent with the results reported in Belov *et al* (2006 *Phys. Rev.* B **73** 033108), which describes subwavelength imaging by an array of metallic wires normal to the interface, the setup considered here may enable the transport of the subwavelength details of a given source through an oblique projection. The array of tilted wires permits the transfer of the electric field component parallel to the wires at the image plane, even when there is no electric field normal to interface, and thus the manipulation of other near-field components (i.e. other wave polarizations) that are not accessible with the usual setup of wires normal to the interface. The emergence of negative refraction due to the extreme anisotropy of structured material is also demonstrated.

[1] Author to whom any correspondence should be addressed.

© IOP Publishing Ltd and Deutsche Physikalische Gesellschaft

Contents

1. Introduction

The effects of diffraction imply that the resolution of classical imaging devices is restricted by the wavelength of light. Conventional lenses cannot resolve two objects that are spaced by a distance inferior to half-wavelength of radiation, because they only operate with the far field of the source, formed by propagating spatial harmonics. The subwavelength information is related to the near-field of the source and is inaccessible by conventional imaging systems, because it is associated with evanescent spatial harmonics that decay exponentially in free space.

During this decade, several approaches were proposed to achieve subwavelength imaging in different frequency regimes [1]–[7]. In particular, it was demonstrated that an array of perfectly conducting wires (wire medium lens) may provide subwavelength resolution up to infrared frequencies [8]–[14]. The operation of such a device is based on the transformation of evanescent harmonics into propagating waves inside a metamaterial slab. This regime is designated by canalization, and becomes possible if the crystal has a flat isofrequency contour and its thickness is equal to an integer number of half-wavelengths (Fabry–Perot condition).

In this paper we study the near-field transport by a wire medium slab formed by tilted wires. The motivation for tilting the wires is that the typical configuration of the wire medium lens (with wires normal to the interface) is polarization sensitive and enables subwavelength imaging of only *p*-polarized waves (magnetic field is parallel to the interface). Here, we demonstrate that due to the increased degrees of freedom, an array of tilted wires may enhance the imaging properties of *s*-polarized waves (electric field is parallel to interface), and thus may enable the transport of electromagnetic field components inaccessible with the setup of [9]. It is suggested that by mechanically rotating the proposed system, so that three different measurements are made, it may be possible to reconstruct all the components of the electromagnetic field. Finally, we show that due to the extreme anisotropy of the material the proposed structure may enable the emergence of negative refraction for some angles of incidence.

The paper is organized as follows. In section 2 we describe a homogenization approach that models the scattering of waves by the wire medium slab (formed by tilted wires). In section 3, the transmission and reflection properties of the metamaterial slab are studied for two

different configurations, using both homogenization theory and full-wave simulations. Next, in section 4 we demonstrate that the proposed system may enable the transport of the near-field components in different scenarios and for different source polarizations. In section 5, we discuss the emergence of negative refraction. Finally, in section 6 the conclusions are drawn.

In this work the fields are assumed monochromatic with time dependence $e^{j\omega t}$.

2. Homogenization model

The structure considered here consists of a set of parallel metallic wires with finite length arranged in a square lattice with period a, as illustrated in figure 1(a). The wires have radius r_w and are oriented along the direction $\hat{\mathbf{u}}_\alpha = \sin\alpha\hat{\mathbf{u}}_y + \cos\alpha\hat{\mathbf{u}}_z$ (forming an angle α with the z-direction) (figure 1(b)), where $\hat{\mathbf{u}}_y$ and $\hat{\mathbf{u}}_z$ are the unit vectors along the coordinate axes. The wires are embedded in a dielectric with relative permittivity ε_h.

The wire medium is characterized by the following dielectric function [15]:

$$\bar{\bar{\varepsilon}}_{\text{eff}} = \varepsilon_h(\hat{\mathbf{u}}_x\hat{\mathbf{u}}_x + \hat{\mathbf{u}}_p\hat{\mathbf{u}}_p + \varepsilon_{\text{eff},\alpha\alpha}\hat{\mathbf{u}}_\alpha\hat{\mathbf{u}}_\alpha)\,, \quad \varepsilon_{\text{eff},\alpha\alpha}(\omega, k_\alpha) = 1 - \frac{\beta_p^2}{\varepsilon_h(\omega/c)^2 - k_\alpha^2}, \tag{1}$$

where the unit vector $\hat{\mathbf{u}}_p = \cos\alpha\hat{\mathbf{u}}_y - \sin\alpha\hat{\mathbf{u}}_z$ is normal to the wires (figure 1(b)), $k_0 = \omega/c$ is the wave number in free space and c is the speed of light in vacuum, $k_\alpha = \mathbf{k}\cdot\mathbf{u}_\alpha$ is the projection of the wave vector $\mathbf{k} = (k_x, k_y, k_z)$ onto the direction of the wires, and β_p is the plasma wave number, which only depends on the lattice period a and on the radius of the wires r_w [15],

$$\beta_p^2 = \frac{2\pi/a^2}{\ln(a/2\pi r_w) + 0.5275}. \tag{2}$$

The wire medium supports three different electromagnetic modes (transverse electromagnetic (TEM) mode, transverse electric (TE) mode and transverse magnetic (TM) mode) [15], in contrast with the usual uniaxial crystals which only support two different plane waves (ordinary and extraordinary waves) [16, 17]. This property is explained by the strong spatial dispersion effects that characterize the wire medium at any frequency, particularly in the long-wavelength limit. The dispersion characteristic for the electromagnetic modes can be found in [18, 19], and the electric field polarization is as follows [18, 19]:

$$\mathbf{E} \sim \frac{\mathbf{k}_\parallel}{|\mathbf{k}_\parallel|} e^{-j\mathbf{k}\cdot\mathbf{r}} \quad \text{(TEM mode)}, \tag{3}$$

$$\mathbf{E} \sim \frac{\mathbf{k}_\parallel \times \hat{\mathbf{u}}_\alpha}{|\mathbf{k}_\parallel \times \hat{\mathbf{u}}_\alpha|} e^{-j\mathbf{k}\cdot\mathbf{r}} \quad \text{(TE mode)}, \tag{4}$$

$$\mathbf{E} \sim \left(\frac{\mathbf{k}_\parallel}{\sqrt{\varepsilon_h}(\omega/c)} + \frac{\varepsilon_h(\omega/c)^2 - k^2}{\varepsilon_h(\omega/c)^2\varepsilon_{\text{eff},\alpha\alpha} - k^2} \frac{k_\alpha}{\sqrt{\varepsilon_h}(\omega/c)} \hat{\mathbf{u}}_\alpha \right) e^{-j\mathbf{k}\cdot\mathbf{r}} \quad \text{(TM mode)}, \tag{5}$$

where $\mathbf{k}_\parallel = \mathbf{k} - \mathbf{k}\cdot\hat{\mathbf{u}}_\alpha\hat{\mathbf{u}}_\alpha$. The magnetic field is given by

$$\mathbf{H} = \frac{1}{\eta_h} \frac{\mathbf{k}}{\sqrt{\varepsilon_h}(\omega/c)} \times \mathbf{E}, \tag{6}$$

where η_h represents the impedance of the host medium.

Next, we briefly sketch the homogenization approach that is used to characterize the reflection and transmission properties of the structure of figure 1 for two different configurations

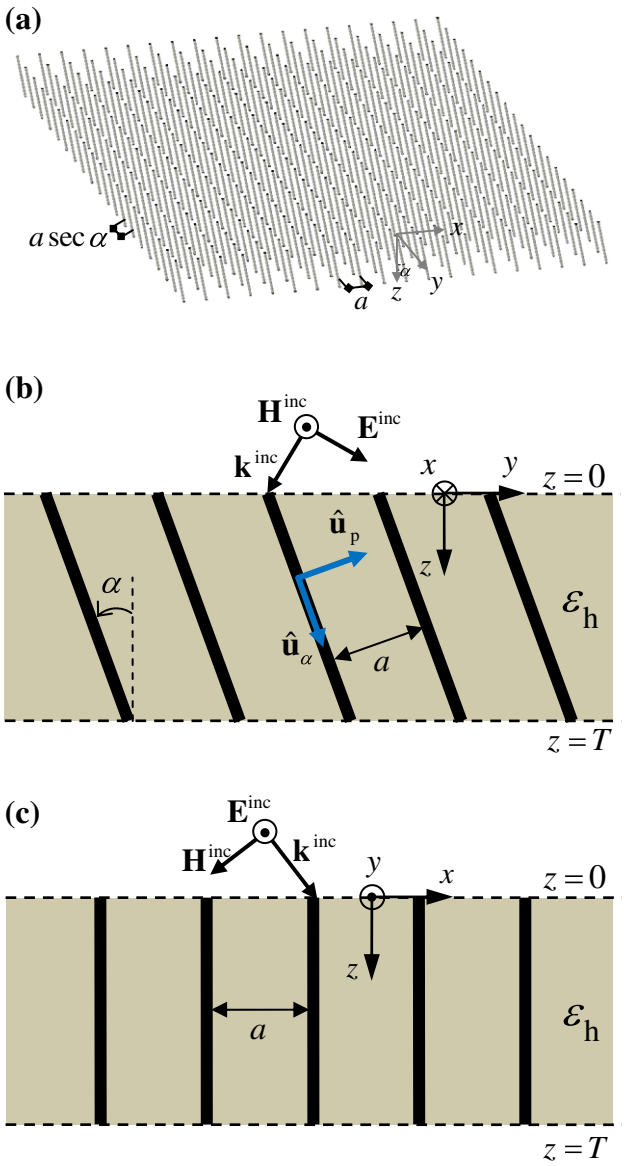

Figure 1. Panel (a) shows the tilted square array of metallic wires. Panels (b) and (c) show the two different cuts of the wire medium substrate. The wires lie in planes parallel to the yoz plane. Panel (b) Configuration I: plane of incidence is the yoz plane and the incident wave has TM-z polarization [$\mathbf{k}^{\rm inc} = (0, k_y, k_z^{\rm inc})$, $\mathbf{H}^{\rm inc} = H\hat{\mathbf{u}}_x$]. Panel (c) Configuration II: plane of incidence is the xoz plane and the incident wave has TE-z polarization [$\mathbf{k}^{\rm inc} = (k_x, 0, k_z^{\rm inc})$, $\mathbf{E}^{\rm inc} = E\hat{\mathbf{u}}_y$].

(figure 1(b) and (c)). The metamaterial slab is formed by wires with length L (the thickness of the slab is $T = L\cos\alpha$). In the first configuration, it is assumed that the incident plane wave has wave vector $\mathbf{k}^{\rm inc} = (0, k_y, k_z^{\rm inc})$ and that the magnetic field is parallel to the interface (the wave is TM with respect to the z-direction). In the second configuration, the incoming wave

propagates in the xoz plane with $\mathbf{k}^{\rm inc} = (k_x, 0, k_z^{\rm inc})$, and the incident electric field is parallel to the interface (the wave is TE with respect to the z-direction).

The total electromagnetic fields for $z < 0$ are such that:

$$\mathbf{E} = \mathbf{E}^{\rm inc} e^{-j\mathbf{k}^{\rm inc}\cdot\mathbf{r}} + \left(\rho_{\rm co}\mathbf{E}^{\rm ref}_{\rm co} + \rho_{\rm cr}\mathbf{E}^{\rm ref}_{\rm cr}\right) e^{-j\mathbf{k}^{\rm ref}\cdot\mathbf{r}}, \tag{7a}$$

$$\mathbf{H} = \mathbf{H}^{\rm inc} e^{-j\mathbf{k}^{\rm inc}\cdot\mathbf{r}} + \left(\rho_{\rm co}\mathbf{H}^{\rm ref}_{\rm co} + \rho_{\rm cr}\mathbf{H}^{\rm ref}_{\rm cr}\right) e^{-j\mathbf{k}^{\rm ref}\cdot\mathbf{r}}, \tag{7b}$$

where $\rho_{\rm co}$ is the reflection coefficient for the co-polarized wave, $\rho_{\rm cr}$ is the reflection coefficient for the cross-polarized wave and $\mathbf{E}^{\rm inc}$, $\mathbf{H}^{\rm inc}$, $\mathbf{E}^{\rm ref}_{\rm co}$, $\mathbf{H}^{\rm ref}_{\rm co}$, $\mathbf{E}^{\rm ref}_{\rm cr}$ and $\mathbf{H}^{\rm ref}_{\rm cr}$ are the incident, reflected co-polarized and reflected cross-polarized, electric and magnetic fields, respectively. The reflected co-polarized and cross-polarized electric fields for each configuration are defined by the following equations:

$$\mathbf{E}^{\rm ref}_{\rm co,config.I} = \mathbf{E}^{\rm ref}_{\rm cr,config.II} = \frac{c}{\omega}\left(\frac{\hat{\mathbf{u}}_z \times \mathbf{k}^{\rm ref}}{|\hat{\mathbf{u}}_z \times \mathbf{k}^{\rm ref}|}\right) \times \mathbf{k}^{\rm ref}, \tag{8a}$$

$$\mathbf{E}^{\rm ref}_{\rm cr,\ config.I} = \mathbf{E}^{\rm ref}_{\rm co,config\ .II} = \frac{\hat{\mathbf{u}}_z \times \mathbf{k}^{\rm ref}}{|\hat{\mathbf{u}}_z \times \mathbf{k}^{\rm ref}|}, \tag{8b}$$

where $\mathbf{k}^{\rm ref}$ is the wave vector associated with the reflected wave. The formulas for the co-polarized and cross-polarized magnetic fields are readily obtained from the Maxwell equations.

Inside the wire medium slab, $0 < z < T$, the fields can be written in terms of the TE, TM and TEM modes supported by the bulk wire medium. Hence, we have the expansions

$$\begin{aligned}\mathbf{E} = {} & A^+_{\rm TE}\mathbf{E}^+_{\rm TE}e^{-j\mathbf{k}^+_{\rm TE}\cdot\mathbf{r}} + A^-_{\rm TE}\mathbf{E}^-_{\rm TE}e^{-j\mathbf{k}^-_{\rm TE}\cdot\mathbf{r}} + A^+_{\rm TM}\mathbf{E}^+_{\rm TM}e^{-j\mathbf{k}^+_{\rm TM}\cdot\mathbf{r}} + A^-_{\rm TM}\mathbf{E}^-_{\rm TM}e^{-j\mathbf{k}^-_{\rm TM}\cdot\mathbf{r}} \\ & + A^+_{\rm TEM}\mathbf{E}^+_{\rm TEM}e^{-j\mathbf{k}^+_{\rm TEM}\cdot\mathbf{r}} + A^-_{\rm TEM}\mathbf{E}^-_{\rm TEM}e^{-j\mathbf{k}^-_{\rm TEM}\cdot\mathbf{r}},\end{aligned} \tag{9a}$$

$$\begin{aligned}\mathbf{H} = {} & A^+_{\rm TE}\mathbf{H}^+_{\rm TE}e^{-j\mathbf{k}^+_{\rm TE}\cdot\mathbf{r}} + A^-_{\rm TE}\mathbf{H}^-_{\rm TE}e^{-j\mathbf{k}^-_{\rm TE}\cdot\mathbf{r}} + A^+_{\rm TM}\mathbf{H}^+_{\rm TM}e^{-j\mathbf{k}^+_{\rm TM}\cdot\mathbf{r}} + A^-_{\rm TM}\mathbf{H}^-_{\rm TM}e^{-j\mathbf{k}^-_{\rm TM}\cdot\mathbf{r}} \\ & + A^+_{\rm TEM}\mathbf{H}^+_{\rm TEM}e^{-j\mathbf{k}^+_{\rm TEM}\cdot\mathbf{r}} + A^-_{\rm TEM}\mathbf{H}^-_{\rm TEM}e^{-j\mathbf{k}^-_{\rm TEM}\cdot\mathbf{r}},\end{aligned} \tag{9b}$$

where $A^{\pm}_{\rm TE,TM,TEM}$ are the unknown amplitudes of the excited modes, $\mathbf{k}^{\pm}_{\rm TE,TM,TEM}$ are the wave vectors of the excited modes [18, 19], $\mathbf{E}^{\pm}_{\rm TE,TM,TEM}$ and $\mathbf{H}^{\pm}_{\rm TE,TM,TEM}$ are defined consistently with equations (3)–(6).

Finally, for $z > T$, the transmitted fields are of the form

$$\mathbf{E} = \left(t_{\rm co}\mathbf{E}^{\rm tr}_{\rm co} + t_{\rm cr}\mathbf{E}^{\rm tr}_{\rm cr}\right) e^{-j\mathbf{k}^{\rm tr}\cdot\mathbf{r}}, \tag{10a}$$

$$\mathbf{H} = \left(t_{\rm co}\mathbf{H}^{\rm tr}_{\rm co} + t_{\rm cr}\mathbf{H}^{\rm tr}_{\rm cr}\right) e^{-j\mathbf{k}^{\rm tr}\cdot\mathbf{r}}, \tag{10b}$$

where $t_{\rm co}$ is the transmission coefficient for the co-polarized wave, $t_{\rm cr}$ is the transmission coefficient for the cross-polarized wave, and $\mathbf{E}^{\rm tr}_{\rm co}$, $\mathbf{H}^{\rm tr}_{\rm co}$, $\mathbf{E}^{\rm tr}_{\rm cr}$ and $\mathbf{H}^{\rm tr}_{\rm cr}$ are the transmitted co-polarized and transmitted cross-polarized electric and magnetic fields, respectively. The transmitted co-polarized and cross-polarized electric fields are defined by expressions analogous to equation (8), with $\mathbf{k}^{\rm ref}$ replaced by $\mathbf{k}^{\rm tr}$ (the wave vector associated with the transmitted wave).

Due to the effects of spatial dispersion [20] (evidenced by the existence of three electromagnetic modes), the usual boundary conditions (continuity of the tangential components

of the electromagnetic field) are insufficient to determine the reflection coefficients ρ_{co} and ρ_{cr}, the transmission coefficients t_{co} and t_{cr} and the six coefficients $A^{\pm}_{TE,TM,TEM}$. An additional boundary condition (ABC) is required at the interface between the homogenized wire medium and the dielectric ($z = 0$ and T). In [18, 19], it was proven that the normal component of the electric field must be continuous at both interfaces, i.e.

$$\mathbf{E} \cdot \hat{\mathbf{u}}_z\big|_{\text{air side}} = \varepsilon_h \mathbf{E} \cdot \hat{\mathbf{u}}_z\big|_{\text{wire medium side}}. \tag{11}$$

Imposing this ABC and the classical boundary conditions, we obtain a 10×10 linear system that can be solved numerically with respect to the unknowns.

When the metallic wires are densely packed (limit $a/L \to 0$ with r_w/a fixed, a being the lattice constant and L the length of the wires) it is possible to use an alternative model to characterize the electromagnetic response of the wire medium. It was shown in [19] that in such circumstances the effect of the TM mode is negligible because its attenuation constant is very large. Thus, the wave propagation in the metamaterial slab can be described solely in terms of the TE and of the TEM modes. Specifically, it was proven in [19] that in the limit $a/L \to 0$ the wire medium behaves as a material with extreme anisotropy with dielectric function of the form [19]

$$\bar{\bar{\varepsilon}}_{\text{eff}} = \varepsilon_h(\hat{\mathbf{u}}_x\hat{\mathbf{u}}_x + \hat{\mathbf{u}}_p\hat{\mathbf{u}}_p + \infty\hat{\mathbf{u}}_\alpha\hat{\mathbf{u}}_\alpha), \tag{12}$$

i.e. the permittivity along the direction of the wire axes is infinitely large. Within the framework of model (12), the material may be regarded as a local material (spatial dispersion effects are negligible when $a/L \to 0$), and thus ABCs are not required.

In the next section, we will compare the transmission and reflection characteristics obtained by using the spatially dispersive homogenization model, with those obtained by using the less rigorous extreme anisotropy model (12), and also with full-wave simulations.

3. Reflection and transmission characteristics

It was shown in previous works [8]–[10] that an array of metallic wires normal to the interface enables the transport of the subwavelength details associated with the component of electric field parallel to the wires (i.e. normal to the interface). The subwavelength information associated with the remaining Cartesian components of the field is not imaged. Consequently, the setup introduced in [9] is polarization sensitive, being transparent to the s-polarized waves (electric field parallel to the interface). Our objective is to study if by tilting the wires it is still possible to capture and propagate the component of the electric field parallel to the wires. In particular, we want to show that by tilting the wires along a suitable direction of space (so that the electric field has a nontrivial projection onto the wires), it is possible to transport the subwavelength information associated with s-polarized waves.

In order to analyze the response of a metamaterial slab when illuminated by p-polarized waves (figure 1(b)) and s-polarized-waves (figure 1(c)), we define the reflection and transmission coefficients relative to the direction parallel to the wires $\hat{\mathbf{u}}_\alpha$:

$$\rho_{\text{eff}} = \frac{\left(\rho_{co}\mathbf{E}^{\text{ref}}_{co} + \rho_{cr}\mathbf{E}^{\text{ref}}_{cr}\right) \cdot \hat{\mathbf{u}}_\alpha}{\mathbf{E}^{\text{inc}} \cdot \hat{\mathbf{u}}_\alpha}, \tag{13}$$

$$t_{\text{eff}} = \frac{\left(t_{co}\mathbf{E}^{\text{tr}}_{co} + t_{cr}\mathbf{E}^{\text{tr}}_{cr}\right) \cdot \hat{\mathbf{u}}_\alpha}{\mathbf{E}^{\text{inc}} \cdot \hat{\mathbf{u}}_\alpha}. \tag{14}$$

Next, for the two configurations of figure 1, we study the dependence of the reflection and transmission coefficients on the direction of the incoming wave, using both the homogenization model and full-wave simulations obtained with the electromagnetic simulator CST Studio Suite™ 2008 [21].

3.1. Configuration I

First we consider configuration I (figure 1(b)) for which the incoming wave propagates in the yoz plane and is TM-z polarized (p-polarization). It is simple to verify that in this case the cross-polarized fields vanish and consequently the cross-polarized coefficients are zero. Hence, equations (13) and (14) reduce to

$$\rho_{\text{eff}} = \frac{\left(\rho_{\text{co}}\mathbf{E}_{\text{co}}^{\text{ref}}\right)\cdot\hat{\mathbf{u}}_{\alpha}}{\mathbf{E}^{\text{inc}}\cdot\hat{\mathbf{u}}_{\alpha}}, \tag{15}$$

$$t_{\text{eff}} = \frac{\left(t_{\text{co}}\mathbf{E}_{\text{co}}^{\text{tr}}\right)\cdot\hat{\mathbf{u}}_{\alpha}}{\mathbf{E}^{\text{inc}}\cdot\hat{\mathbf{u}}_{\alpha}}. \tag{16}$$

In figure 2 the amplitudes of the reflection and transmission coefficients are depicted as a function of the (normalized) transverse component of the wave vector k_y ($k_y = k_0 \sin\theta_{\text{i}}$ for a propagating incoming plane wave, θ_{i} being the angle of incidence). The solid lines are associated with the nonlocal homogenization model, the dashed lines with the extreme anisotropy model, whereas the discrete symbols were obtained with CST Microwave Studio. Clearly, the results for the reflection and transmission coefficients obtained using the three different approaches concur relatively well.

Similar to the case of a slab with wires normal to interface [10], it is seen that when $k_0 L = \pi$, i.e. when the Fabry–Perot condition is verified, the absolute value of the transmission coefficient in the direction parallel to the wires (t_{eff}) is very close to unity (even for evanescent waves), confirming that the tilted wire medium (figure 1) operates in a canalization regime and is capable of transporting the electric field component parallel to wires, even when the wires are tilted. The extreme anisotropy condition corresponds to the ideal situation: at the Fabry–Perot resonance the effective reflection coefficient vanishes, whereas the amplitude of the transmission coefficient is unity for all spatial harmonics (including evanescent waves).

It should be noted that the Fabry–Perot resonance is determined by the length of the wires L, and not by the thickness of the slab T ($T = L\cos\alpha$). For grazing incidence, i.e. when $k_y \approx k_0$, the effective transmission coefficient exhibits an abrupt decay, and the canalization effect is not observed. It is also interesting to note that when the length of the slab is slightly larger than the Fabry–Perot resonance length the effect of reflections is weaker.

Naturally, the behavior of the effective reflection and transmission coefficients is sensitive to variations in the frequency of operation (or equivalently to variations in the electrical length of the wires). In figure 3, the effective reflection and transmission coefficients are shown for wires with length larger than half-wavelength. In the same manner, as for the usual configuration of the wire medium slab [8]–[10], the transmission coefficient for evanescent waves becomes weaker, except in the vicinity of the point $k_y = k_0$ where some resonance is visible.

On the other hand, for wire lengths smaller than half-wavelength (or equivalently for frequencies below the Fabry–Perot resonance), the transmission and reflection coefficients are greatly enhanced by the excitation of guided modes propagating along the y-direction of the

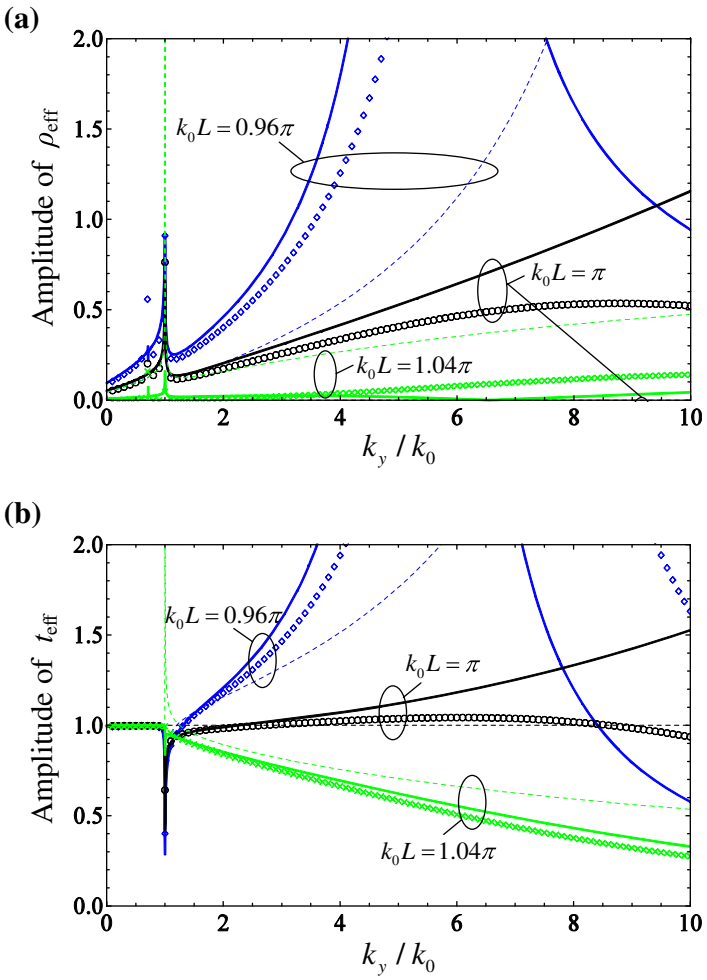

Figure 2. Amplitude of the reflection (panel (a)) and transmission (panel (b)) coefficients as a function of the normalized transverse wave vector k_y for configuration I (figure 1(b)), for a fixed normalized frequency $k_0a = 0.1$ and different wire lengths L. The permittivity of the dielectric substrate is $\varepsilon_h = 1$, the radius of the wires $r_w = 0.05a$ and the tilt angle is $\alpha = 45^\circ$. Solid lines: nonlocal homogenization model. Dashed lines: extreme anisotropy model. Discrete symbols: numerical results obtained with CST Microwave Studio [21]. Notice that the reflection coefficient calculated using the extreme anisotropy model is exactly zero at the Fabry–Perot resonance ($k_0L = \pi$), and thus the corresponding curve in panel (a) is coincident with the horizontal axis.

slab, as can be seen in figure 4, consistent with the results of [10]. It may be noticed in figures 2–4 that the effective reflection coefficient exhibits resonant behavior at $k_y = 0.7k_0$, more specifically when the direction of the incoming wave is parallel to the wires. In this case it is clear that $\mathbf{E}^{\text{inc}} \cdot \hat{\mathbf{u}}_\alpha = 0$ and thus the co-polarized reflection coefficient vanishes $\rho_{\text{co}} = 0$. However, ρ_{eff} is different from zero because both the numerator and denominator of formula (15) vanish. This explains the abrupt variations in ρ_{eff} seen in figures 2–4 around $k_y = 0.7k_0$, which evidently have little physical meaning since the actual reflected electric field is negligible.

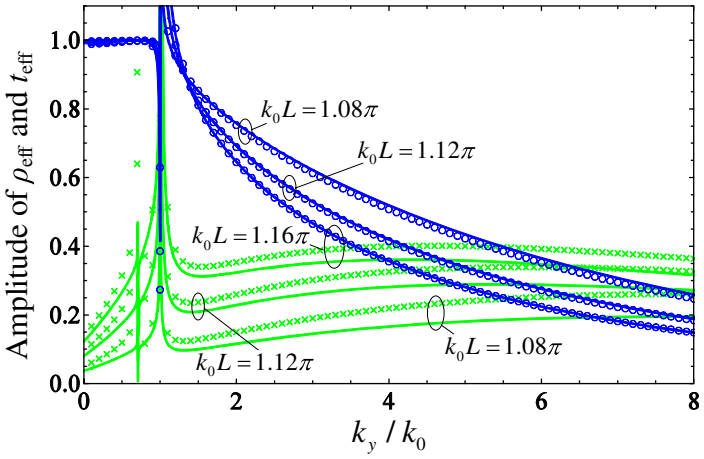

Figure 3. Amplitude of the reflection (green) and transmission (blue) coefficients as a function of the normalized transverse component of the wave vector k_y for configuration I, for a fixed normalized frequency $k_0a = 0.1a$ and different wire lengths L. The permittivity of the dielectric substrate is $\varepsilon_{\text{h}} = 1$, the radius of the wires is $r_{\text{w}} = 0.05a$ and the tilt angle is $\alpha = 45^\circ$. Solid lines: nonlocal homogenization model. Discrete symbols: numerical results obtained with CST Microwave Studio [21].

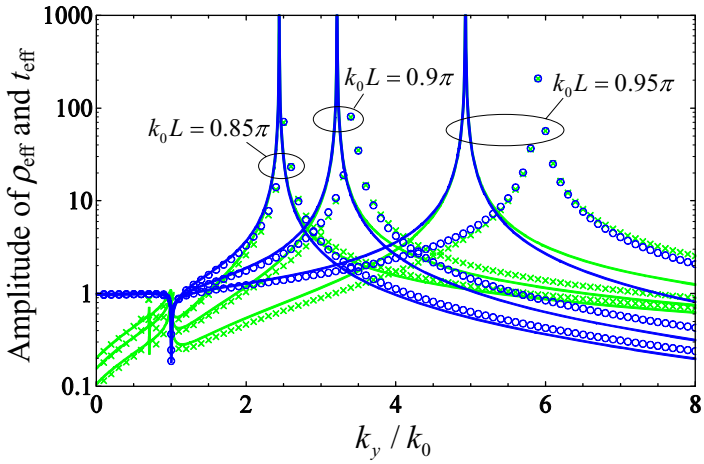

Figure 4. Similar to figure 3 but for length of wires below the Fabry–Perot condition.

An interesting property of the system under study is that the phase of the transmission coefficient may vary significantly with the angle of incidence. This is shown in figure 5, where the phase of the transmission coefficient is depicted for different tilt angles α. For straight wires, $\alpha = 0^\circ$, the phase is practically equal to -180° for the whole range of k_y. However, when α is decreased and the wires are tilted, the phase of the effective transmission coefficient varies linearly with k_y/k_0, with a slope $k_0L\sin\alpha$ (assuming without loss of generality that the host material is air). This property can be understood by noting that the metallic wires perform pixel-to-pixel imaging, and therefore the transfer function of the system (determined

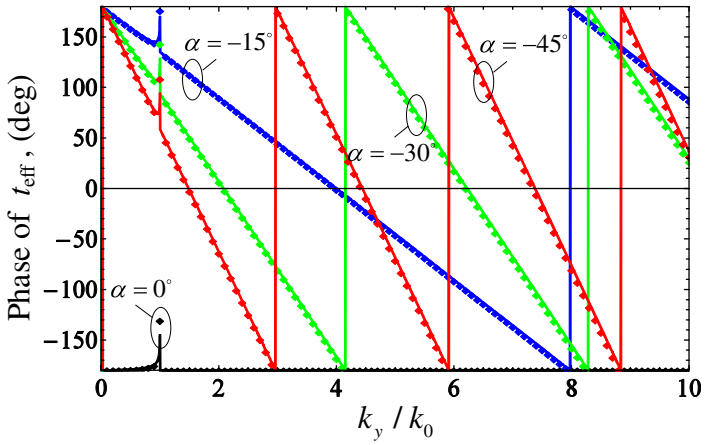

Figure 5. Phase of the transmission coefficient as a function of the normalized transverse component of the wave vector k_y for different tilt angles. Configuration I, with permittivity of the dielectric substrate $\varepsilon_h = 1$, radius of the wires $r_w = 0.05a$ and $L = \lambda/2$. Solid lines: nonlocal homogenization model. Discrete symbols: numerical results obtained with CST Microwave Studio [21].

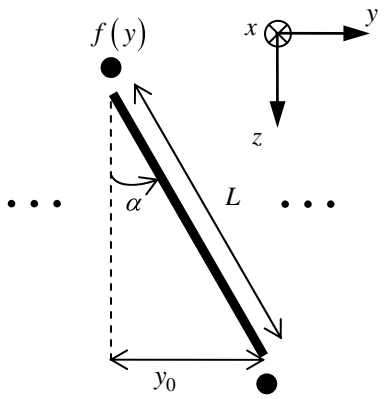

Figure 6. Pixel-to-pixel imaging by a generic wire.

by the transmission coefficient) should correspond to a spatial shift of the image at the output plane $f(y) \rightarrow f(y - y_0)$ (see figure 6), with $y_0 = L \sin\alpha$. But a spatial shift corresponds in the spectral (Fourier) domain to a phase shift,

$$f\,(y - y_0) \overset{\text{F}}{\rightarrow} \tilde{f}\,(k_y)\,\mathrm{e}^{\mathrm{j}k_y y_0} \tag{17}$$

and this justifies the results of figure 5, and the fact that the phase of the transfer function strongly depends on k_y.

3.2. Configuration II

Next, we study the reflection and transmission properties of the tilted wire medium for configuration II (figure 1(c)). Now the incoming wave propagates in the xoz plane and is

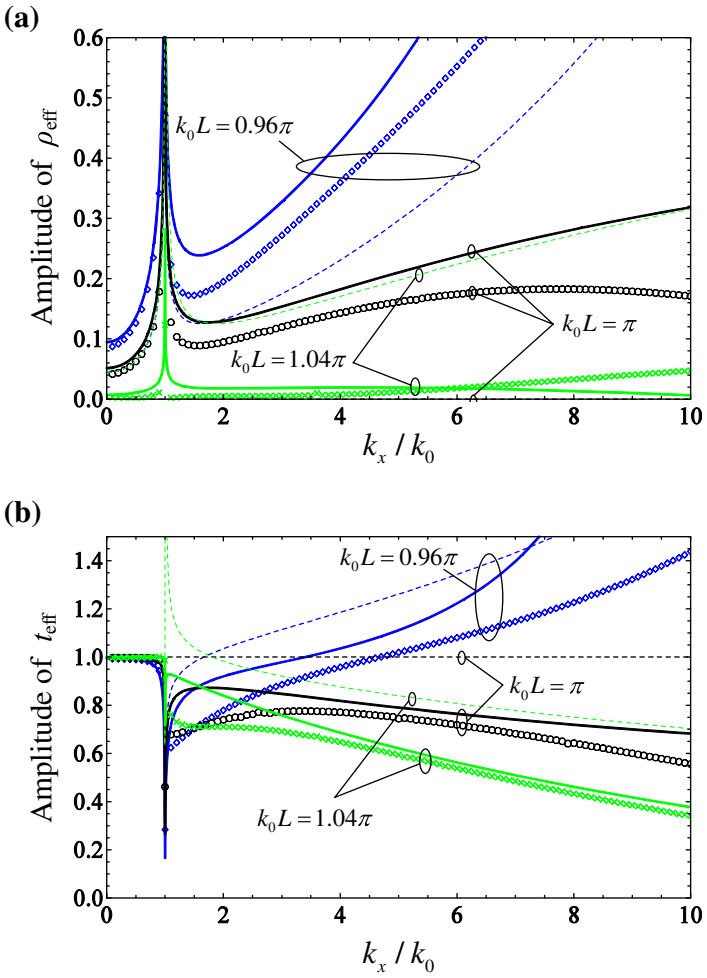

Figure 7. Amplitude of the reflection (panel (a)) and transmission (panel (b)) coefficients as a function of the normalized transverse wave vector k_x for configuration II (figure 1(c)), for a fixed normalized frequency $k_0a = 0.1$ and different wire lengths L. The permittivity of the dielectric substrate is $\varepsilon_{\rm h} = 1$, the radius of the wires is $r_{\rm w} = 0.05a$ and the tilt angle is $\alpha = 45^\circ$. Solid lines: nonlocal homogenization model. Dashed lines: extreme anisotropy model. Discrete symbols: numerical results obtained with CST Microwave Studio [21]. Notice that the reflection coefficient calculated using the extreme anisotropy model is exactly zero at the Fabry–Perot resonance ($k_0L = \pi$) and thus the corresponding curve in panel (a) is coincident with the horizontal axis.

TE-z polarized (s-polarization). In this configuration the cross components of the reflection and transmission coefficients ($\rho_{\rm cr}$ and $t_{\rm cr}$, respectively) may be different from zero.

We calculated the reflection and transmission coefficients as a function of the transverse component of the wave vector, k_x ($k_x = k_0 \sin\theta_{\rm i}$ for a propagating incoming plane wave) using the nonlocal homogenization model, the extreme anisotropy model (equation (12)), and full-wave simulations [21]. The obtained results for the amplitude of the reflection and transmission coefficients are represented in figure 7(a) and (b), respectively, for configurations where the length of the wires is close to the Fabry–Perot resonance length ($L = \lambda_0/2$). As in section 3.1,

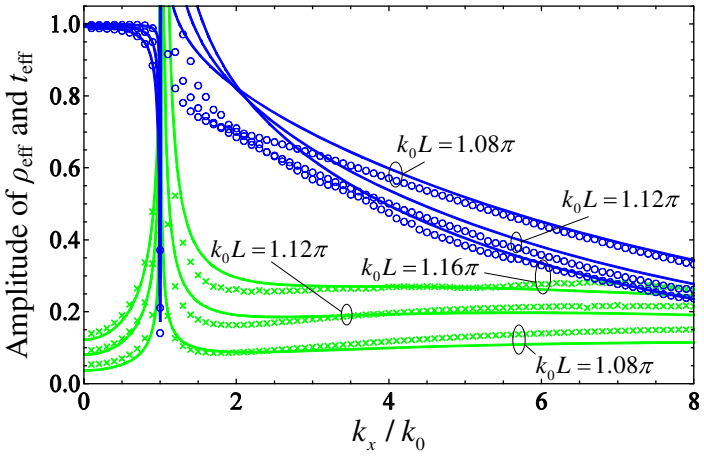

Figure 8. Amplitude of the reflection (green) and transmission (blue) coefficients as a function of the normalized transverse component of the wave vector k_x for configuration II, for a fixed normalized frequency $k_0a = 0.1$ and different wire lengths L. The permittivity of the dielectric substrate is $\varepsilon_h = 1$, the radius of the wires is $r_w = 0.05a$ and the tilt angle is $\alpha = 45^\circ$. Solid lines: nonlocal homogenization model. Discrete symbols: numerical results obtained with CST Microwave Studio [21].

also here the agreement between the coefficients calculated using the three different methods is very reasonable.

In figure 7 it is seen that the behavior of the reflection and transmission coefficients for this configuration is similar to that of configuration I (see figure 2). In particular, when the Fabry–Perot condition is verified ($k_0L = \pi$), the amplitude of the transmission coefficient (for the electric field component parallel to the wires) is still close to unity for all spatial harmonics (including evanescent harmonics). Thus, these results confirm, indeed, that even though for this configuration there is only electric field parallel to interface, it is still possible to operate the tilted wire medium in the canalization regime [8], and transport the component of the electric near-field parallel to the wires.

As in configuration I, the extreme anisotropy condition (achievable in the limit of very densely packed wires, $a/L \to 0$) corresponds to the ideal situation where at the Fabry–Perot resonance $|t_{\text{eff}}| = 1$ and $\rho_{\text{eff}} \approx 0$ for all spatial harmonics.

As in section 3.1, the response of the system may change when the wires length (or the frequency of operation) is altered. For $k_0L > \pi$ (figure 8) the amplitude of the effective reflection coefficient tends to increase with frequency, whereas the amplitude of the effective transmission coefficient tends to decrease. In the vicinity of $k_y \approx k_0$ resonances arise due to the propagation of guided modes along the x-direction of the slab [10].

The effect of guided modes in the reflection and transmission characteristics is particularly important for wire lengths below half-wavelength ($k_0L < \pi$), originating sharp resonances in the transfer functions (figure 9), and causing the selective amplification of spatial harmonics. As discussed in [10] the effect of these guided modes in imaging applications may be critical since they tend to distort the image created by the source with high-frequency noise.

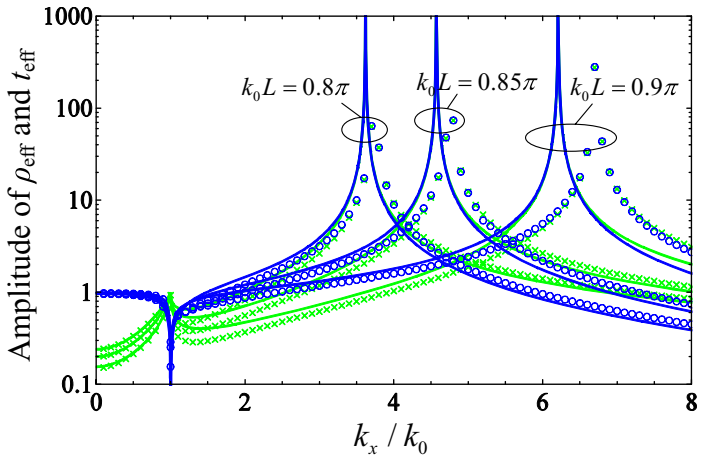

Figure 9. Similar to figure 8 but for length of wires below the Fabry–Perot condition.

4. Near-field transport

In order to verify the results discussed in the previous section and evaluate the potentials of near-field transport by the tilted wire medium, several numerical simulations of the structure were performed for both configurations (figure 1(b) and (c)). These results are presented and discussed next.

4.1. Configuration I

In the first example, we consider a setup based on configuration I (figure 1(b)), and formed by an array of 20×20 metallic wires tilted by an angle of 45°. This structure was illuminated by the wave diffracted by a perfectly conducting screen with two narrow slits (figure 10) under plane wave incidence ($\mathbf{E}^{\text{inc}} = E\hat{\mathbf{u}}_y$, $\mathbf{H}^{\text{inc}} = H\hat{\mathbf{u}}_x$). The wave diffracted by each slit mimics closely the field radiated by a magnetic line current directed along the direction of the slit [13], and thus the polarization of the wave that impinges on the wire medium slab is predominantly transverse magnetic (TM-z; p-polarization). Using CST Microwave Studio [21] we have calculated the y- and z-components of the electric field (i.e. the components with nontrivial projections along the wires direction), at the input and output planes. The x-component of the electric field is negligible for this configuration.

The length of the wires ($L = 15$ cm) is tuned so that the first Fabry–Perot condition occurs at 1 GHz. By scaling the structure, it is possible to obtain similar results at terahertz and infrared frequencies [13]. The results of the simulation at the design frequency are presented in figure 11.

It is clear from figure 11(a) and (b) that the imaging properties of the y-component of the electric field are excellent and that the two slits are perfectly resolved in the image plane. An identical situation occurs with the z-component of the electric field as can be seen in figure 11(c) and (d). Therefore, consistently with the homogenization model, the tilted wire medium enables, indeed, the transfer of the subwavelength details of the image from the front interface to the back interface, through an oblique projection.

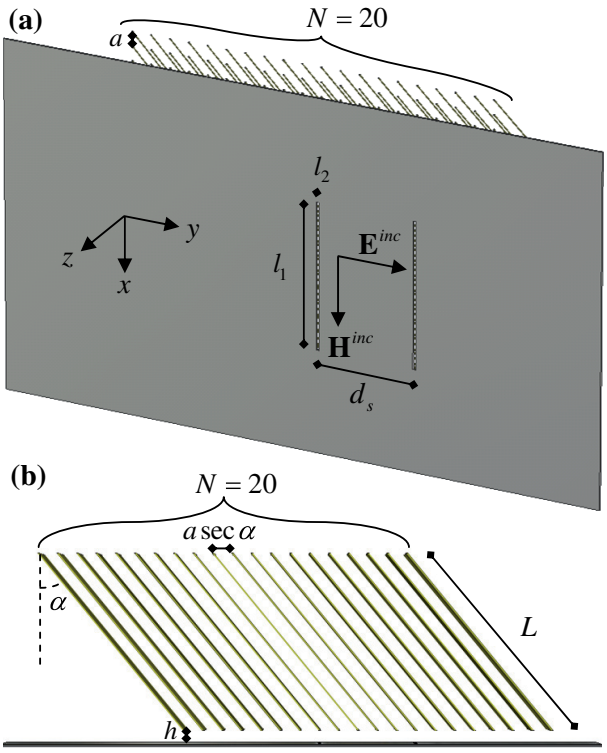

Figure 10. Geometry of the finite-sized slab of tilted wires. The image is created by a metallic screen with two narrow slits that is illuminated by a plane wave: (a) perspective view, and (b) top view. The wires stand in free space ($\varepsilon_h = 1$), the length of the wires $L = 15$ cm and are tilted by an angle $\alpha = 45^\circ$, the period of the lattice $a = 1$ cm, and the radius of the wires $r_w = 0.5$ mm. The screen is at a distance of $h = 8$ mm from the front interface of the slab, and the slits have dimensions $l_1 = 10$ cm and $l_2 = 2$ mm. The slits are separated by $d_s = 7.07$ cm.

At frequencies lower than the design frequency (figure 11(e) and (f) for 0.95 GHz), and consistent with the results of [10], the imaging properties are deteriorated, and the two slits are hardly discernible, even at the front interface (figure 11(e)). This happens due to strong reflections that occur for frequencies below the design frequency, mainly due to the excitation of guided modes (see figure 4).

At higher frequencies, e.g. 1.05 GHz (figure 11(g) and (h)), the imaging properties are still very good and subwavelength imaging is still achieved. This could be expected from the results of figures 2 and 3. For frequencies higher than 1.05 GHz it is expected that the imaging properties will be progressively deteriorated due to the decrease of the transmission coefficient for high-frequency spatial harmonics (figure 3).

4.2. Configuration II

In the second example, we consider a setup related to configuration II (figure 1(c)), with a source that radiates s-polarized waves (electric field perpendicular to the plane of incidence). Specifically, we study a problem where two electric line sources fed by currents in opposition of phase (and infinitely extended along the y-direction) are placed at a distance d_1 from the

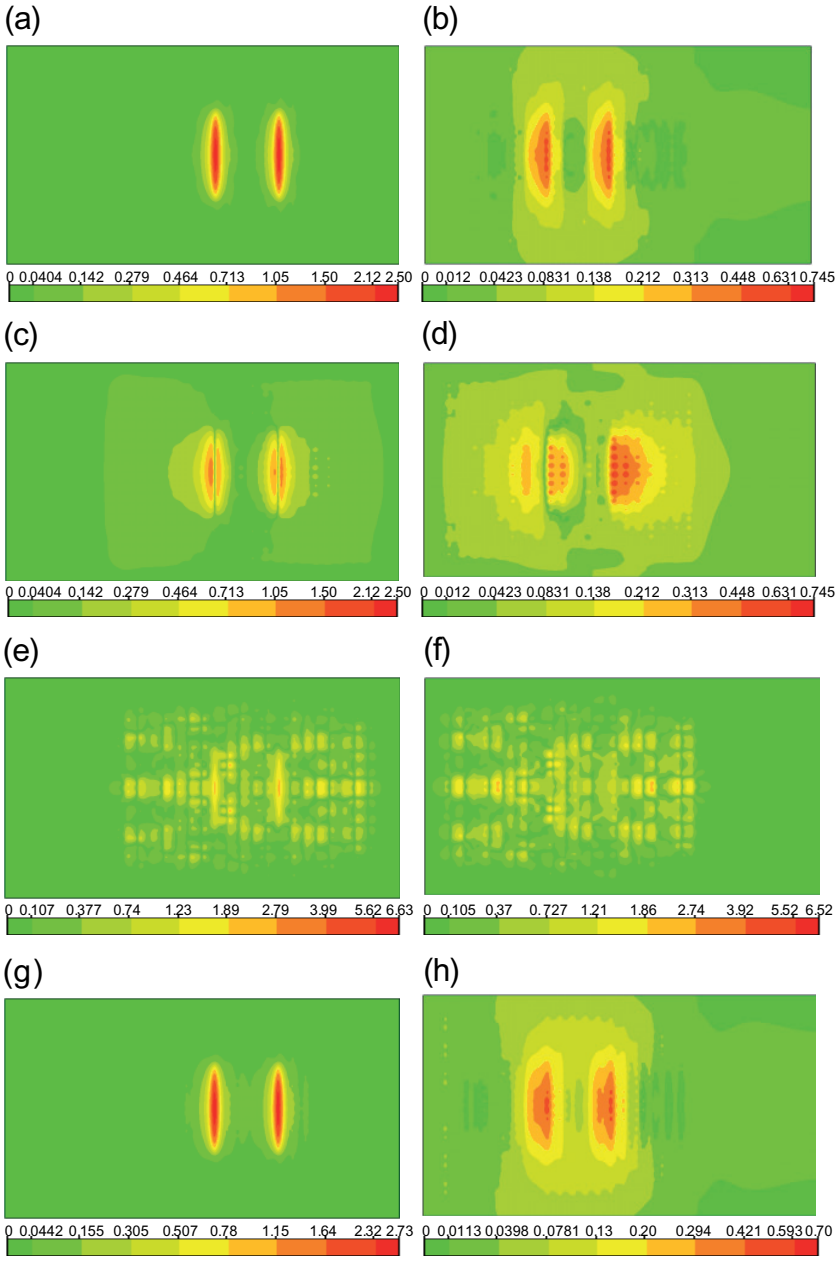

Figure 11. Distribution of electric field (V m^{-1}): (a), (c), (e), (g) at the source plane, at distance $h/2 = 0.4a$ from both the front interface and source; (b), (d), (f), (h) at the image plane, at distance $h/2 = 0.4a$ from the back interface; (a) and (b) absolute value of the y-component of the electric field $|E_y|$ at 1 GHz; (c) and (d) absolute value of the z-component of the electric field $|E_z|$ at 1 GHz; (e) and (f) absolute value of the y-component of the electric field $|E_y|$ at 0.95 GHz; (g) and (h) absolute value of the y-component of the electric field $|E_y|$ at 1.05 GHz.

front interface (see the inset of figure 12). The electric field radiated by the line sources is of the form $E_y = E_0 \frac{1}{4\mathrm{j}}(H_0^{(2)}(k_0\rho_1) - H_0^{(2)}(k_0\rho_2))$, where E_0 is some constant that depends on the line current, ρ_1 and ρ_2 are the radial distances relative to the sources, and $H_0^{(2)}$ is the Hankel function

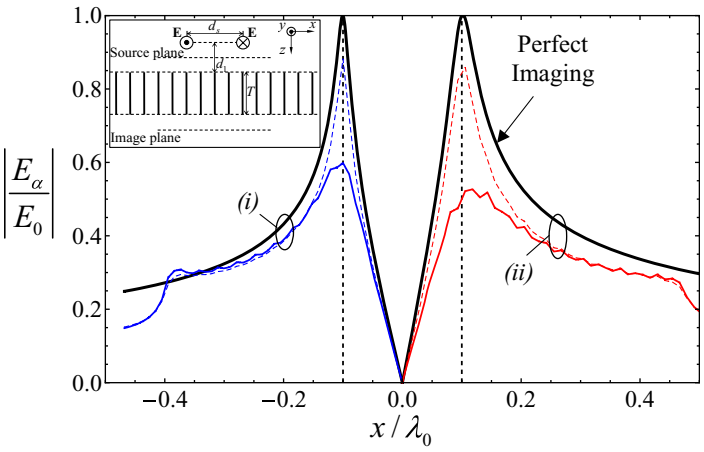

Figure 12. Amplitude of the normalized electric field component parallel to the metallic wires at the image and source planes. The inset represents the geometry of the problem: two electric line sources are fed by currents in opposition of phase. The line sources are placed at a distance d_1 above the tilted wire medium slab and are separated by a distance d_s. The source and image planes are located at a distance $d_1/2$ from the front and back interfaces, respectively. The width of the structure in the x-direction is W. Parameters of the problem: (i) (left-hand side panel, $x < 0$) $L = \lambda_0/2$, $a = L/(10\pi)$, $r_w = 0.05a$, $\varepsilon_h = 1$, $\alpha = 45^\circ$, $d_1 = 0.016\lambda_0$, $d_s = 0.2\lambda_0$ and $W \approx 0.8\lambda_0$ (50 rows of wires in the x-direction); (ii) (right-hand side panel, $x > 0$) $L = \lambda_0/2$, $a = L/(5\pi)$, $r_w = 0.05a$, $\varepsilon_h = 1$, $\alpha = 45^\circ$, $d_1 = 0.032\lambda_0$, $d_s = 0.2\lambda_0$ and $W \approx 0.95\lambda_0$ (30 rows of wires in the x-direction). Solid black line: perfect imaging (i.e. field profile at the source plane when the array of wires is removed); dashed lines: field profile at the source plane; solid colored lines: field profile at the image plane. The vertical black dashed lines represent the position of the sources.

of second kind and order zero. Using the method of moments (MoM), taking into account in this manner all the fine details of the microstructure of the artificial material, we have calculated the electric field profile along the direction of the wires, at the source and image planes. In the MoM simulation the artificial material slab was assumed periodic along the y-direction, and finite along the x-direction with width W.

In figure 12 the amplitude of the normalized electric field along the direction of the wires (E_α) is represented at the source and image planes for a metamaterial slab formed by tilted wires ($\alpha = 45^\circ$) with length $L = \lambda_0/2$ (Fabry–Perot resonance), and different lattice constants. In both simulations ((i) and (ii)) we only show the field profiles for one of the sources, since it is obvious that by symmetry $|E_\alpha|$ is an even function of x. The field profiles on the left-hand side panel of figure 12 ($x < 0$) correspond to a simulation with $a = L/(10\pi)$. It is seen that, despite the distance between the sources being as small as $d_s = 0.2\lambda_0$, the field profiles at image plane (solid line) and source plane (dashed line) are similar except in the close vicinity of the line sources, where the field amplitude has a steep variation. Such abrupt variations of the near-field are associated with very high-frequency spatial harmonics. It is expected that if the density of wires is increased the transported field will mimic more closely the field at the source plane.

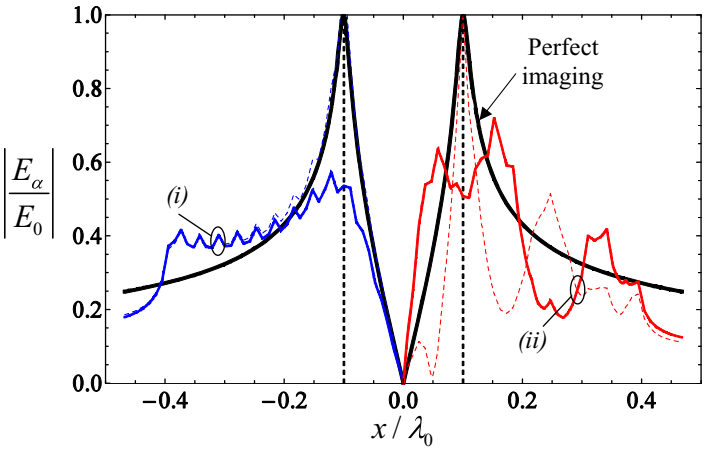

Figure 13. Amplitude of the normalized electric field component parallel to the metallic wires at the image and source planes. Parameters of the problem: (i) (left-hand side panel, $x < 0$) $L = 0.54\lambda_0$, $a = L/(10.8\pi)$, $r_w = 0.05a$, $\varepsilon_h = 1$, $\alpha = 45^\circ$, $d_1 = 0.016\lambda_0$, $d_s = 0.2\lambda_0$ and $W \approx 0.8\lambda_0$ (50 rows of wires in the x-direction); (ii) (right-hand side panel, $x > 0$) $L = 0.45\lambda_0$, $a = L/(9\pi)$, $r_w = 0.05a$, $\varepsilon_h = 1$, $\alpha = 45^\circ$, $d_1 = 0.016\lambda_0$, $d_s = 0.2\lambda_0$ and $W \approx 0.8\lambda_0$ (50 rows of wires in the x-direction). The legend is as in figure 12.

Indeed, it is well known that the resolution of the considered system is approximately equal to the lattice constant [10, 13].

The field profiles on the right-hand side panel of figure 12 correspond to a metamaterial slab with a lower density of wires ($a = L/(5\pi)$) (the distance between the two sources and the front interface is also doubled as compared to the first scenario). As could be expected, the imaging quality is slightly deteriorated, consistent with the fact that a is increased, and thus the resolution of the system is worsened.

The described full-wave results confirm the findings of section 3, and further demonstrate that a tilted wires slab (figure 1) can indeed transfer the subwavelength details of the source, restoring the component of the electric field parallel to the wires at the image plane, even when there is no electric field normal to the input interface. Notice that in the present configuration the sources radiate s-polarized waves.

At the source plane, it is possible to detect a slight decrease of the amplitude of the electric field E_α in comparison to the situation in which the array of tilted wires is removed. This is completely consistent with the results of section 3 (figure 7(a)), and is explained by the fact that the amplitude of the reflection coefficient ρ_{eff} may be significant at the considered frequency ($k_0 L = \pi \Rightarrow L = \lambda_0/2$), while its phase is equal to π for the evanescent spatial harmonics, which causes the incident and reflected fields to interact destructively.

In figure 13 we represent the profile of E_α for the situations where the dimensions of the tilted wire medium slab are not tuned according to the Fabry–Perot resonance, i.e. the length of wires is slightly larger (left-hand side panel) and smaller (right-hand side panel) than half-wavelength.

When $L = 0.54\lambda_0$ ($x < 0$) the sources become more difficult to distinguish at the image plane, consistent with the results of figure 8, which predict a decrease in the amplitude of the

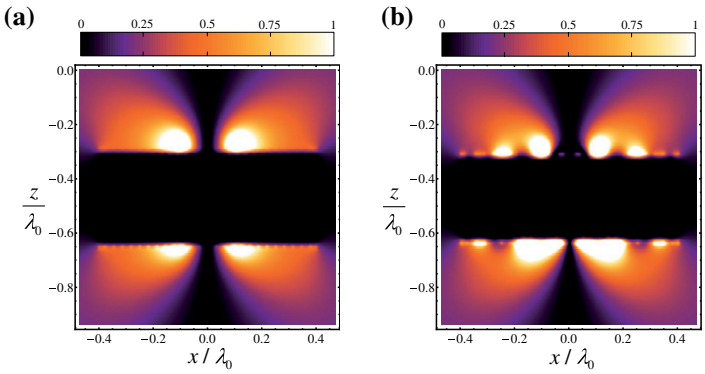

Figure 14. $|E_\alpha|^2$ for an array of tilted wires with the same geometry as in figure 12: (a) same parameters as figure 12(i) and (b) same parameters as figure 13(ii).

transmission coefficient. As discussed before, if the length of the wires is further increased it is expected that the imaging properties are progressively deteriorated and eventually the sources may become indistinguishable. At the source plane, the amplitude of the electric field is higher than at $L = 0.5\lambda_0$ (figure 12(i)). This is also consistent with reflection characteristic of the system (see figures 7(a) and (8)), given that the amplitude of ρ_{eff} for $L = 0.54\lambda_0$ is lower than for $L = 0.5\lambda_0$.

When $L = 0.45\lambda_0$ ($x > 0$) the imaging properties are very poor, and the sources are hardly perceptible. Clearly, the field profile is completely corrupted by high-frequency noise. As discussed in section 3, the reason for this phenomenon is related to the excitation of the guided modes propagating along the x-direction of the slab, which cause the amplification of some spatial harmonics (see figure 9).

In order to further characterize the imaging properties of the system, we depict in figure 14 density plots of $|E_\alpha|^2$ in the xoz plane, for the same configurations as in figure 12(i) (left-hand side panel) and figure 13(ii) (right-hand side panel). Notice that inside the metamaterial slab the component of the electric field parallel to the metallic wires practically vanishes, $E_\alpha \approx 0$, consistent with the boundary condition observed by the electric field on the surface of a good conductor.

Figure 14(a) shows that when the wire length is tuned according to the Fabry–Perot condition, $L = 0.5\lambda_0$, the two sources are clearly resolved at the image plane. On the other hand, when $L = 0.45\lambda_0$ (figure 14(b)), the near-field has many secondary peaks, associated with guided modes, as discussed before.

The results of this section suggest a very interesting possibility [22]. Indeed, since for a fixed orientation of the metallic wires it is possible to transport and restore the electric field component parallel to the wires (i.e. the component $E_\alpha = \mathbf{E} \cdot \hat{\mathbf{u}}_\alpha$), then by rotating the wire medium lens along the z-axis it is possible to change the orientation of the wires ($\hat{\mathbf{u}}_\alpha$), and consequently we can capture the projection of the electric field along a different direction of space. In particular, if the slab of tilted wires is sequentially rotated three times by 120° around the z-axis, we can measure the projections of the electric field along three directions of space that are not coplanar. Since the three-dimensional space is completely determined by three linearly independent vectors, it is possible to reconstruct all the near-field Cartesian components of the

electric field at the image plane by making only three measurements [22]. The magnetic field may then be easily computed from the electric field using the Stratton–Chu formulas [23]. This approach clearly requires that the wires are tilted with respect to the interface, and cannot be implemented using the standard configuration of [9].

5. Negative refraction

One interesting feature of the studied metamaterial is that it may enable an unusual and peculiar form of negative refraction for certain angles of incidence. Indeed, since the array of metallic wires performs pixel-to-pixel imaging, it follows that for any angle of incidence θ_i the angle of transmission inside the metamaterial slab is invariant and equal to $\theta_t = \alpha$. Such a property should be clear from the geometry of the metamaterial slab (figure 1(b)), and may also be shown to be fully consistent with the extreme anisotropy model (12), as detailed below. The property $\theta_t = \alpha$ clearly implies that for a certain range of incident angles, the group velocity (which is parallel to the Poynting vector) will suffer negative refraction. In fact, it is well known that negative refraction does not require a negative index [1], [24]–[27] and may be obtained using anisotropic materials [28].

To demonstrate this property we have studied the transmission of a Gaussian beam through a metamaterial slab. The plane of incidence is the yoz plane and the incoming wave is TM-z polarized. In the simulations the artificial material slab is assumed periodic along the x-direction, and finite along the y-direction (geometry is similar to that of figure 1(b)). The width of the structure is taken equal to $W \approx 9\lambda_0$ (80 rows of wires spaced by $\sqrt{2}a$ along the y-direction). The Gaussian beam is characterized by the following magnetic field distribution $H_x \approx H_0 \exp(-\mathrm{j}k_0 z') \exp[-y'^2/(w_0^2 - 2\mathrm{j}z'/k_0)]/\sqrt{1 - 2\mathrm{j}z'/k_0 w_0^2}$, where k_0 represents the wave number, w_0 is the beam waist and y' and z' are associated with a coordinate system such that z' varies along the direction of propagation of the beam.

As explained in [19] and discussed in section 2, when the wires are densely packed ($a/L \to 0$) the TEM mode becomes the dominant propagating mode and the material is characterized by extreme anisotropy. The dispersion characteristic for the TEM mode is given by [19]:

$$\mathbf{k} \cdot \hat{\mathbf{u}}_\alpha = \pm \frac{\omega}{c} \sqrt{\varepsilon_h}, \quad \text{i.e} \quad k_z \cos\alpha + k_y \sin\alpha = \pm \frac{\omega}{c} \sqrt{\varepsilon_h}. \tag{18}$$

Thus, the isofrequency contours correspond to two planes normal to the direction of the wires $\hat{\mathbf{u}}_\alpha$, as represented in figure 15(a). The Poynting vector is normal to the isofrequency contours, and thus it follows that the transmitted angle is necessarily such that $\theta_t = \alpha$, as anticipated in the beginning of this section.

Using the method of moments, we have calculated the field transmitted across the metamaterial slab for $\theta_i = 45^\circ$ (figure 15(c)) and for $\theta_i = 60^\circ$ (figure 15(d)), assuming that the Gaussian beam is characterized by $2w_0 = 4\lambda_0$. The density plots of the squared amplitude of the electric field $|\mathbf{E}|^2$ are depicted in figure 15(c) and (d), clearly demonstrating the emergence of negative refraction. In figure 15(c) there is no reflected wave and consequently the system is well matched to free space. Indeed, our simulations suggest that for incident beams propagating along a direction perpendicular to $\hat{\mathbf{u}}_\alpha$ the system is always perfectly matched, even if the length of the wires does not coincide with multiples of $\lambda_0/2$ (Fabry–Perot condition). For other angles of incidence the effects of reflection may not be negligible, as illustrated in figure 15(d).

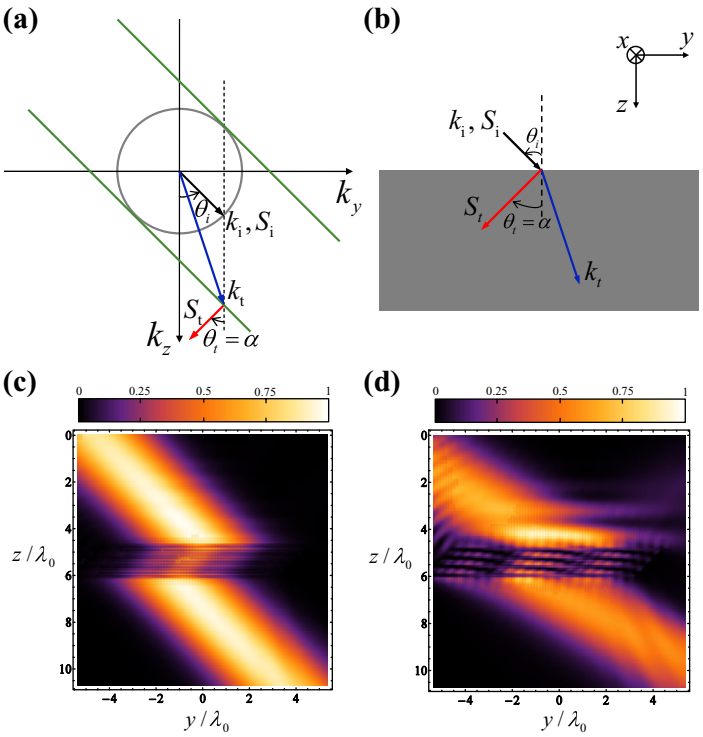

Figure 15. (a) The isofrequency contour of the TEM mode supported by the tilted wire medium with $\varepsilon_h = 1$, $\alpha = -45^\circ$ and $r_w = 0.05a$ (green lines), as well as the isofrequency contour in the air region (gray circle). The transmitted wave vector k_t (blue arrow) is determined by the conservation of the tangential component of the wave vector k_y, whereas the Poynting vector S_t (red solid arrow) is normal to the isofrequency curves and oriented along the increasing frequencies. (b) Schematic representation of negative refraction of a TM-z incident wave incident on the tilted wire medium. (c) and (d) Plots of the squared amplitude of the electric field. (c) The length of the wires is $L = 2\lambda_0$, the lattice period is $a = L/(8\pi)$ and the Gaussian beam is incident in the slab with an angle $\theta_i = 45^\circ$. (d) The length of the wires is $L = 1.875\lambda_0$, the lattice period is $a = 2L/(15\pi)$ and the Gaussian beam is incident in the slab with an angle $\theta_i = 60^\circ$.

Obviously, the refraction properties depend on the orientation of the wires. Negative refraction of the Poynting vector only occurs when the angle of incidence verifies $\theta_i \alpha < 0$, otherwise the Poynting vector (group velocity) suffers positive refraction.

6. Conclusion

In this paper, we studied the potentials of near-field transport by an array of tilted wires. It was shown, as a generalization of the results of [8]–[14], that the considered system may enable the transport of the subwavelength details associated with electric field component parallel to the wires through an oblique projection. Such property implies that it is possible to image the fields created by s-polarized sources, for which the electric field is parallel to the interfaces of the structure. This is an important advance since the standard configuration of [9] does not

interact with *s*-polarized waves. It was suggested that by mechanically rotating the array of metallic wires successively by 120°, it may be possible to retrieve all the electric field Cartesian components, independent of the wave polarization. Finally, it was discussed that due to the extreme anisotropy of the wire medium, it may be possible to observe negative refraction in some circumstances. It is expected that the described results may be useful in sensing and imaging at terahertz and infrared frequencies, where metals may still behave as good conductors.

Acknowledgments

This work was funded by Fundação para Ciência e a Tecnologia under project PDTC/EEA-TEL/71819/2006. TM acknowledges financial support by Fundação para a Ciência e a Tecnologia under the fellowship SFRH/BD/37876/2007. The authors gratefully acknowledge fruitful discussions with Dr P A Belov.

References

[1] Pendry J B 2000 *Phys. Rev. Lett.* **85** 3966
[2] Zhang X 2004 *Phys. Rev.* B **70** 205102
[3] Freire M J and Marques R 2005 *Appl. Phys. Lett.* **86** 182505
[4] Fang N, Lee H, Sun C and Zhang X 2005 *Science* **308** 534
[5] Salandrino A and Engheta N 2006 *Phys. Rev.* B **74** 075103
[6] Smolyaninov I I, Hung Y J and Davis C C 2007 *Science* **315** 1699
[7] Freire M J, Marques R and Jelinek L 2008 *Appl. Phys. Lett.* **93** 231108
[8] Belov P A, Simovski C R and Ikonen P 2005 *Phys. Rev.* B **71** 193105
[9] Belov P A, Hao Y and Sudhakaran S 2006 *Phys. Rev.* B **73** 033108
[10] Belov P A and Silveirinha M G 2006 *Phys. Rev.* E **73** 056607
[11] Ikonen P, Simovski C R, Tretyakov S, Belov P and Hao Y 2007 *Appl. Phys. Lett.* **91** 104102
[12] Shevts G, Trendafilov S, Pendry J B and Sarychev A 2007 *Phys. Rev. Lett.* **99** 053903
[13] Silveirinha M G, Belov P A and Simovski C R 2008 *Opt. Lett.* **33** 1726
[14] Belov P A, Zhao Y, Tse S, Ikonen P, Silveirinha M G, Simovski C R, Tretyakov S, Hao Y and Parini C 2008 *Phys. Rev.* B **77** 193108
[15] Belov P A, Marqués R, Maslovski S I, Nefedov I S, Silveirinha M, Simovsky C R and Tretyakov S A 2003 *Phys. Rev.* B **67** 113103
[16] Yariv A and Yeh P 1984 *Optical Waves in Crystals: Propagation and Control of Laser Radiation* (New York: Wiley)
[17] Morris I and Kline K 1965 *Electromagnetic Theory and Geometrical Optics* (New York: Interscience)
[18] Silveirinha M G 2006 *IEEE Trans. Antennas Propag.* **54** 1766–80
[19] Silveirinha M G, Fernandes C A and Costa J R 2008 *New J. Phys.* **10** 053011
[20] Agranovich V and Ginzburg V 1966 *Spatial Dispersion in Crystal Optics and the Theory of Excitons* (New York: Wiley-Interscience)
[21] CST Studio Suite™ 2008 (http://www.cst.com)
[22] Belov P A private communication
[23] Jackson J D 1998 *Classical Electrodynamics* (New York: Wiley)
[24] Shelby R A, Smith D R and Schultz S 2001 *Science* **292** 77–9
[25] Parazzoli C G, Greegor R B, Li K, Koltenbah B E C and Tanielian M 2003 *Phys. Rev. Lett.* **90** 107401
[26] Houck A A, Brock J B and Chuang I L 2003 *Phys. Rev. Lett.* **90** 137401
[27] Valentine J, Zhang S, Zentgraf T, Ulin-Avila E, Genov D A, Bartal G and Zhang X 2008 *Nature* **455** 376–9
[28] Silin R A 2003 *13th Int. Crimean Conf. Microwave and Telecommunication Technology (CriMiCo'2003) (Sevastopol, Ukraine, 8–12 Sept.)* pp 379–81